Available online at www.sciencedirect.com
SCIENCE DIRECT®
Planetary and Space Science 52 (2004) 1169–1175
Planetary and Space Science
www.elsevier.com/locate/pss

First observations of the Na exosphere of Mercury with the high-resolution spectrograph of the 3.5M Telescopio Nazionale Galileo

Cesare Barbieri[a,*], Stefano Verani[a], Gabriele Cremonese[b], Ann Sprague[c], Michael Mendillo[d], Rosario Cosentino[e], Donald Hunten[c]

[a]*Department of Astronomy, University of Padova, I-35122 Padova, Italy*
[b]*Astronomical Observatory of Padova, INAF, Italy*
[c]*Lunar and Planetary Laboratory, University of Arizona, Tucson, AZ 85721, USA*
[d]*Center for Space Physics, Boston University, MA 02215, USA*
[e]*Telescopio Nazionale Galileo, INAF, Italy*

Received 16 September 2003; received in revised form 14 June 2004; accepted 6 July 2004

Abstract

Analysis of three spectra of the exosphere of Mercury in the Na-D lines are presented. Spectra were secured with the high-resolution spectrograph (SARG) of the 3.5 M Telescopio Nazionale Galileo (TNG, located on the Roque de los Muchachos, Canaries) on the evenings of August 23 and 24, 2002. Spectra have resolution $R = 115\,000$; the slit length was 26.7''. The Na column abundances range from 4.3 to 19.7×10^{10} atoms/cm^2 with the highest abundances being close to the illuminated limb. Our observations at true anomaly angles (TAA) from 171°to 174°show the traces of the emission lines to be strongly peaked at the illuminated limb, supportive of recent modeling that shows thermal desorption to be a strong factor in determining the distribution of Na about the planet.

Keywords: Mercury; Planetary exospheres; Na emission atmospheres; High-resolution planetary spectroscopy

1. Introduction

The existence of the atmosphere around Mercury was discovered by the Mariner 10 spacecraft, which revealed UV emissions of three atomic elements: H, He and O (Broadfoot et al., 1976). Three other elements (Na, K, and Ca) were later discovered with ground-based observations (Potter and Morgan, 1985; Potter and Morgan, 1986; Bida et al., 2000, respectively). Due to the low density (of about $n = 10^5$ atoms/cm^3, $P = 10^{-12}$ bar, on the dayside), the atmosphere is collisionless, i.e., the mean-free path of the atoms is longer than the value of the scale height H of the atmosphere (cf. Chamberlain and Hunten, 1987). Therefore, the whole atmosphere is comparable with an exosphere having the exobase coincident with the planet's surface.

The lifetime for the species in the exosphere is ruled by the interaction with the interplanetary medium. Photoionization is the fastest loss mechanism of the neutral atmosphere: the ionized atoms are driven away from the planet by the solar wind, or aimed back to the surface along the lines of Mercury's magnetic field. To maintain the exosphere, the lost atoms must be replaced by some source mechanisms. Processes of endogenic and exogenic origin are supposed to act in repopulating the exosphere. The expected sources of Na include thermal, photon, and electron-stimulated desorption, ion and chemical sputtering, vaporization of regolith and of projectiles following micro-meteoritic impacts (cf. McGrath et al., 1986, Hunten and Sprague, 1997).

*Corresponding author. Fax: +39-498278245.
E-mail address: barbieri@pd.astro.it (C. Barbieri).

0032-0633/$ - see front matter © 2004 Elsevier Ltd. All rights reserved.
doi:10.1016/j.pss.2004.07.013

As gas-phase collisions are negligible, each constituent of Mercury's atmosphere forms an exosphere having different parameters (T, H, n) with respect to the other species. This means that it is possible to follow the evolution of a particular exospheric component without taking into account the others. Exospheric atoms are liberated from the surface with a supra-thermal energy (i.e. with $T_{gas} > T_{surf}$), which depends on the nature of their source mechanism. They can gravitationally escape from the planet (escape velocity = 4.3 km/s), or go into a ballistic orbit which will re-encounter the planet's surface. After a bounce, the atoms can stick to the surface, or bounce again into another ballistic orbit with a different energy, closer to the temperature of the surface, until they are photoionized or readsorbed by the surface (cf. Hunten et al., 1988). The number and the path of the bounces is determined by the nature of the gas–surface interactions, by the lifetime of the neutral atom in the exosphere, and of course by the gravity and radiation pressure. As the atoms can perform several bounces, it is expected that a thermal component is formed, even if the source was supra-thermal, like on the Moon. A thermal component is also liberated from the surface when temperatures are high and the lifetime on the surface is short. At Mercury the thermal component should be the dominant one, because of the higher temperature and greater gravity (cf. Hunten and Sprague, 1997). Indeed, a measurement of the temperature of the Na component via high-resolution spectroscopy was performed by Killen et al. (1999a). They found the presence of two components, a supra-thermal one (1500 K) and another one (600 K) much closer to the surface's temperature.

Following the discoveries of Na and K at Mercury, many ground-based observations have provided the following information regarding their distribution and time variation:

- rapid time variations in the intensity of the exosphere, not correlated with changes in solar activity (e.g. Sprague et al., 1997, Potter et al., 1999),
- enhancements of sodium emission over known geological features on Mercury's surface (Caloris Basin, the Kuiper Murasaki crater complex), and over regions which show radar-bright spots, associated with regions of fresh excavation features on the side of Mercury not imaged by Mariner 10 (Sprague et al., 1998),
- a sodium comet-like tail streaming in the anti-sunward direction with variable abundance and extent (Potter et al., 2002).

Source mechanisms for Na have long been debated. Sprague et al. (1997) found a strong diurnal variation in the emission of Na and K, with a large enhancement in the morning. They conclude that a recycling mechanism is at work, such that some photoionized atoms are driven back to the surface along the lines of the magnetosphere, then neutralized and adsorbed to the surface in the night hemisphere, then released back in the exosphere with the morning illumination. A similar morning-side enhancement has also been observed in the data of Potter (2003, Pers. comm.). Enhancements of K over Caloris Basin and Na over the radar-bright spots were interpreted by Sprague et al. (1998) to be further evidence that diffusion and thermal desorption from surface materials is a primary source. On the other hand, time variations in the abundance of Na and spottiness of the emissions observed in imaging were interpreted to be evidence for charged particle sputtering by Potter and Morgan (1990). A later data set showing changes in Na emissions from the northern to southern latitudes was interpreted by Potter et al. (1999) as evidence for the effects of space weather on the distribution and time variation of Na.

Several models of Mercury's Na exosphere have explored the distribution of Na around the planet under the influence of selected physical processes known to be working in the vicinity of Mercury. Some of these are charged particle sputtering (Killen et al., 1999b), radiation acceleration (Ip, 1990; Smyth and Marconi, 1995), ion implant followed by diffusion and thermal evaporation (Sprague, 1992). A more holistic approach including charged particle sputtering, photo desorption, and thermal desorption using a constant source of micrometeoritic bombardment generated Na has recently been published (Leblanc and Johnson, 2003). The Leblanc and Johnson approach resulted in unique distributions of Na about the planet as a function of true anomaly angle (TAA). The model predicted the Na tail at the TAA observed by Potter et al. (2002).

To provide more data to help understand the phenomena described above, we have undertaken observations with the SARG/TNG. The advantages of using the TNG in this context come from the good collecting aperture, from the outstanding image quality of the site and of the telescope, and from the excellent performances of the SARG in terms of efficiency and resolution. This paper presents the results obtained in the first, largely exploratory, attempt to reach this goal. We judge the results promising enough to plan a program of observations for the next several years. Not only do we hope to clarify the relative role of source mechanisms but we also hope to provide a useful data bank for the forthcoming space missions MESSENGER and BepiColombo.

2. Observations and data reduction

The SARG has been equipped with a Na filter specifically for this purpose of studying diffuse Na in

Solar System objects, because it allows to keep a long slit (26.7 arcsec) on the sky by removing order overlapping. The main characteristics of the spectrograph are given in Table 1.

For further information on SARG, see http://www.pd.astro.it/sarg/. The observations discussed here were carried out on two evenings: 23 and 24 Aug 2002 between 19:00 and 20:00 UT, i.e. during daytime or with the Sun just below the horizon, the minimum elevation of the TNG being 13.5°. To save read-out time, the slit was 2×-binned in the spatial direction making the effective spatial pixel of 0.64 arcsec. The evening of the 23rd was the best in terms of sky transparency and seeing quality.

Mercury and Venus were both near eastern elongation, permitting us to obtain, sequentially and essentially at the same air mass, spectra of Mercury, and Venus across the terminator as null reference for Na emission, and of Spica for flux and point spread function (PSF) calibration. Fig. 1 shows an example of each spectrum, and Fig. 2 the PSF of Spica.

Fig. 3 shows on the same scale the planet and the slit, here in PA = 90°. The Sun is in the upper right corner. Relevant geometric and illumination parameters for our observations are given in Table 2.

Reference spectra (flat fields, bias, dark current, Th–Ar reference lamp) were taken both before and after Mercury's observations and used with the Interactive Reduction and Analysis Facility (IRAF) to prepare the images for analysis using the standard techniques of spectral image reduction. Particular care was adopted in subtracting the diffuse light and the Mercury continuum, in order to obtain the two emission lines from the exosphere. Fig. 4 shows sample spectra from Mercury showing the Na D2 and D1 emission lines on the short-wavelength side of the solar Fraunhofer reflected from Mercury's surface. Also shown are a reflected solar spectrum and an enlarged portion of the Mercury spectrum showing the D2 emission line and the estimated continuum which was removed from the data in order to obtain the uncontaminated emission lines.

Table 1
Instrumentation parameters

Spectrograph resolution	115 000
Slit length and width	26.7 × 0.40 arcsec
Pixel dimension and scale	0.022 A, 0.32 arcsec
CCD dimension	2K × 4K pixels

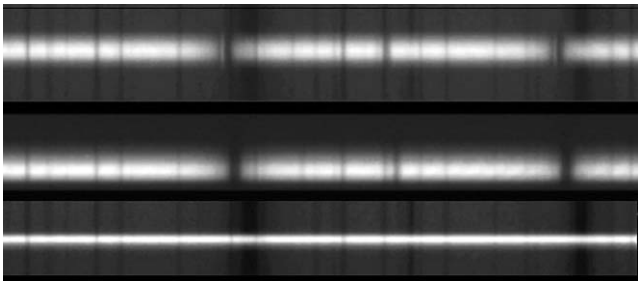

Fig. 1. Spectra of Mercury (top), Venus across the terminator (middle), and Spica. On Mercury, the D2 (5890 Å) and D1 (5896 Å) lines are clearly visible in emission inside the broad Na Fraunhofer absorptions seen in the reflected continuum from Mercury surface.

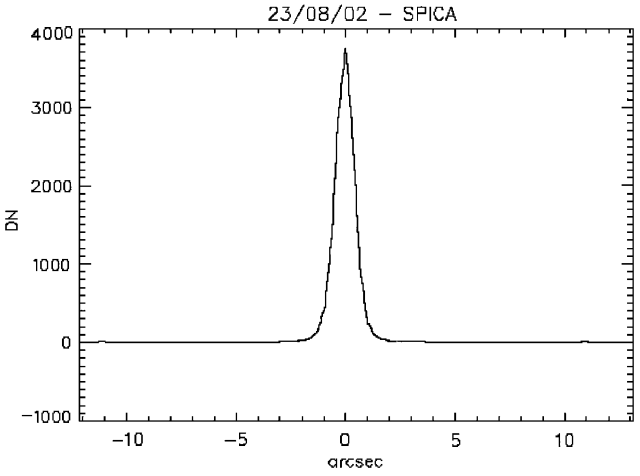

Fig. 2. Profile of Spica during the night of the 23rd. The FWHM was 1.0".

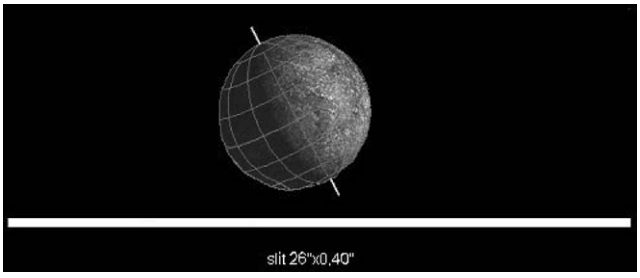

Fig. 3. Mercury and slit (to scale, here shown parallel to PA = 90°). North is up, East to the left.

Table 2
Geometric and illumination parameters

	23 Aug. 2002	24 Aug. 2002
UT	19:34	19:47, 19:49
Heliocentric distance (AU)	0.464866	0.465744
Phase angle	71.0	72.6
Exposure time	30 s	30, 60 s
Diameter (arcsec)	6.3	6.4
Heliocentric Doppler shift (m)	34.4	24.8
Sub-Earth longitude, latitude (degrees)	148.6, 6.5	153.5, 6.6
True anomaly (degrees)	171	174

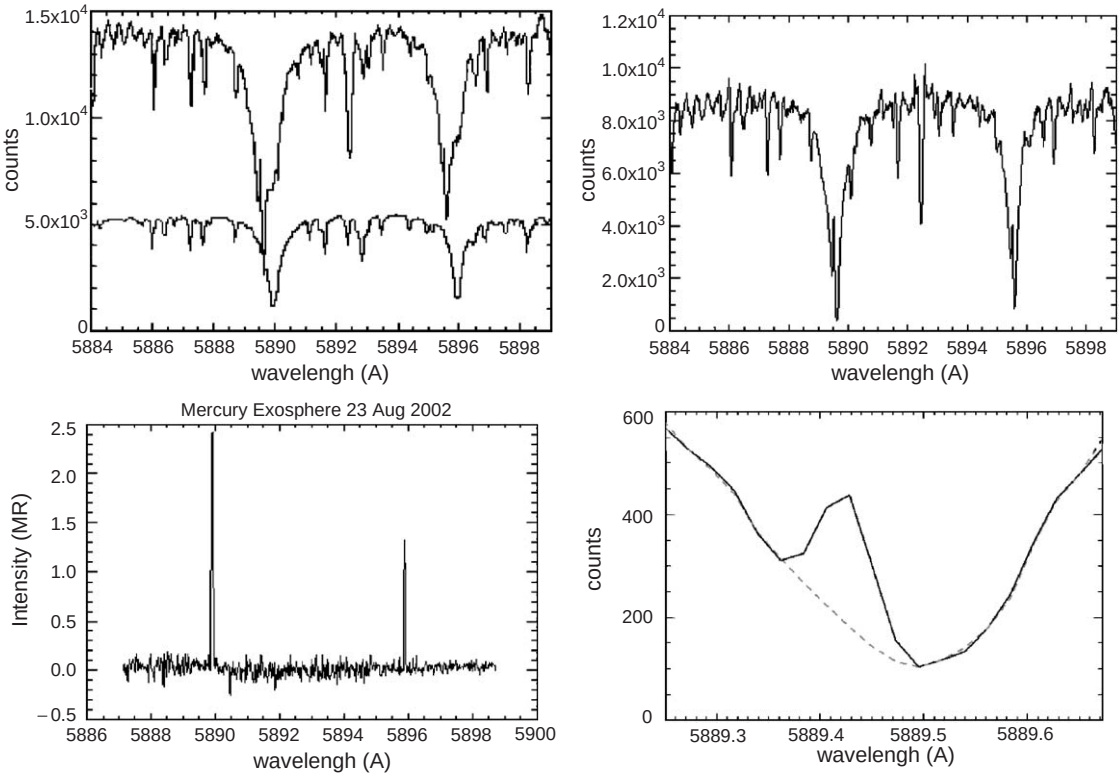

Fig. 4. Upper left: Mercury + sky + diffuse light (upper line) and sky + diffuse light only (bottom line). Upper right: after sky and diffuse light subtraction, the solar reflected continuum and the exospheric D1 and D2 emission are left. Bottom panel: left, after solar continuum removal; right, continuum estimate under D2.

3. Data analysis and results

The position angle (PA) of the slit was at a different value for each of the three spectra presented here, namely PA 90°, 152°, and 118°, respectively. An equatorially aligned slit corresponds to PA 118°. Fig. 5 shows the traces of instrumental data numbers (DNs) along the slit for the continuum, along with a seeing smeared model of the trace across the slit, and for the D2 and D1 lines. The purpose of the seeing smeared model trace is two-fold. First, it provides a measure of the atmospheric "seeing" during the exposure because it can be compared directly to the continuum trace along the slit. Second, it provides a Hapke rough-reflectance surface model (Hapke, 1986) composed of the rough reflectance (Rr) at each location in the smeared surface grid. The grid size can be chosen to represent the parameters of the spectrograph (in this case a spatial pixel of 0.32 arcsec binned × 2, namely 0.64 arcsec). The Hapke Rr can then be used to absolutely calibrate the data using an average of the maximum values from the continuum at a wavelength close to the sodium D lines. We have used the method of Sprague et al. (1997).

For estimating the seeing, we generated several models of each spectrum, then extracted the Rr corresponding to the location of the slit at the time of observation. By plotting the model trace along the slit on the same graph as the actual data, it was possible to get a good estimate of the seeing at the time of the exposure, as shown by the dotted lines in Fig. 5.

We then partitioned the DNs of the D2 and D1 emission along the slit into sectors that are reasonable, given the size of the planet and the actual seeing smear of the image. In these three slit spectra we chose three sectors along the slit for individual conversion to column abundance. With the aid of the Hapke model of the planet, for each exposure we determined the approximate distance of the slit sector in units of fraction of a radius from the center of the planet. From this we also estimated the approximate longitude and latitude of the central portion of the slit sector under analysis. The radiative transfer program accounts for illumination and emission geometry and seeing smear (Hunten and Wallace, 1993; Sprague et al., 1997). For spectral images of excellent seeing and higher spatial resolution, it will be necessary to account for changing surface albedo beneath the slit in the absolute calibration of the slit sectors before conversion of emission DNs to column abundances (Domingue et al., 1997).

Table 3 shows g-factors, Rr, and calibration factors for the three spectra presented in this paper. We use the standard definitions of all the parameters, common in

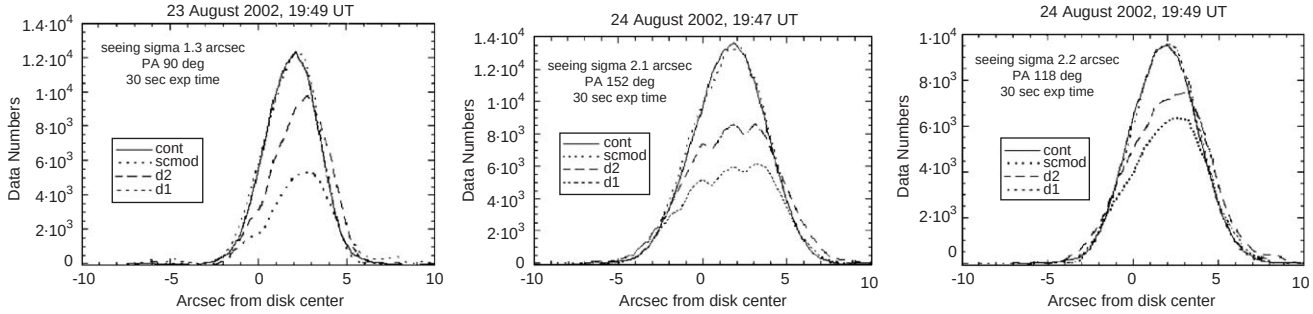

Fig. 5. DN along the slit are shown for all three spectral images presented in this paper. DNs for the continuum are obtained from 1 pixel in the wavelength dimension (0.022 arcsec) and 2 pixels (0.64 arcsec) in the spatial direction. For the D2 and D1 emission line traces, DNs are from 7 pixels (0.154 arcsec) in the spectral and 2 pixels (0.64 arcsec) in the spatial dimension. Also shown (dotted line, scmod) is the trace across the seeing smeared Hapke model for each spectrum.Left: Model indicates good atmospheric seeing ($\sigma = 1.3$ arcsec) for day 1. The slit was oriented 28°with respect to the equator, with the slit being North of the equator coming across the terminator, crossing the equator and going slightly South on the sunlit limb. The emission is offset from the continuum toward the illuminated limb of the planet. Center: The slit was oriented 62°with respect to the equator with the left-hand side being South East in the sky, or coming from the South across the right side of the planet across the terminator, across the equator and going North toward the bright limb. The continuum is fitted reasonably well with $\sigma = 2.1$ arcsec. The contrast of the smooth continuum to the bumpy D2 and D1 emission indicated patchy Na emission. This is discussed in the text.Right: The slit was oriented along the planet's equator, the left-hand side being the night side of the planet. While the emission lines show brighter emission over the bright limb than the terminator, the seeing smear of the continuum ($\sigma = 2.2$ arcsec) does not exhibit the same behavior. This is discussed in the text.

Table 3
Absolute calibration parameters

	Exp. time (s)	Doppler shift (m)	$g1$ (s^{-1})	$g2$ (s^{-1})	Hapke Rr	Cal. factor (kR s DN^{-1})
23 Aug. 19:49	30	34.4	1.7	2.7	0.0101	1.6
24 Aug. 19:47	30	24.8	1.5	2.5	0.0078	1.1
24 Aug. 19:49	60	24.8	1.5	2.5	0.0074	3.1

airglow work detailed in Hunten et al. (1956) and Chamberlain and Hunten (1987). From the observed D2/D1 intensity ratios, it is evident that the Na exosphere is optically thick.

Table 4 gives the approximate locations of the slit sectors, the absolutely calibrated brightness and the vertical column abundance for each emission line.

4. Discussion

The column abundances found in this new observing campaign are very consistent with those of previous observers (cf. Potter and Morgan, 1986; Sprague et al., 1997). The mid-afternoon and late-afternoon portions of the illuminated disk were not available during these observations, but we explored the possibility of a diurnal effect in the data by calculating the densities in the early a.m., mid-a.m. and mid-day sectors (see Table 4). As can be seen in Table 4, the range of locations and the samplings of data from North to South is scant, but we plot the column abundances as a function of fraction of radius from disk center to see if any strong North–South asymmetry is exhibited. A large scatter of equatorial values is observed. There is no statistically significant difference between the mid-a.m. and the mid-day sectors, while the early a.m. sector exhibits slightly lower abundances in accordance with the results of Sprague et al. (1997). These results are also plotted in Fig. 6.

5. Interpretations and conclusions

We have demonstrated that we are well equipped to make high-quality observations using the TNG of Mercury's Na exosphere. Our results of these first observations give column abundances and distribution of Na consistent with those of previous observers. Although our abundances show considerable scatter as they are obtained from many locations on the disk and the number of points is small, the column abundances and the distribution of the Na about the planet are consistent with the predictive modeling of Leblanc and Johnson (2003), who found that column abundances are highest in a band around the sunlit limb at TAA = 181° (see Plate 3, pag. 272). The true anomaly of our observations varies from 171°to 174°. The emission

Table 4
Abundances

	Location				Brightness (kR)		Column abundance (atoms cm^{-2} units of 10^{10})	
	X (E–W)	Y (N–S)	~ lat (deg)	~ long (deg)				
	(fraction of radius from disk center)							
23 Aug. 19:49					D2	D1	D2	D1
early a.m.	−0.29	0.16	12	160	86.4	65.2	5.82	5.69
early a.m.	0.00	0.00	6	150	179.3	102.7	8.81	6.86
mid-a.m.	0.30	−0.21	−2	135	342.3	200.5	13.2	10.6
mid-day	0.76	−0.41	−18	105	489.0	277.1	15.5	10.3
mid-day	0.90	−0.44	−25	75	498.8	285.2	18.9	10.6
24 Aug. 19:47								
early a.m.	−0.25	−0.25	−10	160	148.2	114.0	9.63	9.76
early a.m.	0.00	0.0	6	150	242.8	185.8	13.3	13.9
mid-a.m.	0.30	0.2	15	140	285	201.8	12.1	12.0
mid-a.m.	0.60	0.4	30	125	322.6	225.7	12.7	11.9
mid-day	0.72	0.65	40	85	311.2	231.4	14.4	12.8
24 Aug. 19:49								
early a.m.	−0.30	0.00	6	160	180.7	144.8	14.3	14.0
mid-a.m.	0.10	0.00	6	145	289.2	237.5	17.4	16.4
mid-a.m.	0.60	0.00	3	110	365.8	316.2	18.9	17.2
mid-day	0.95	0.00	0	85	381.3	325.5	19.6	18.8

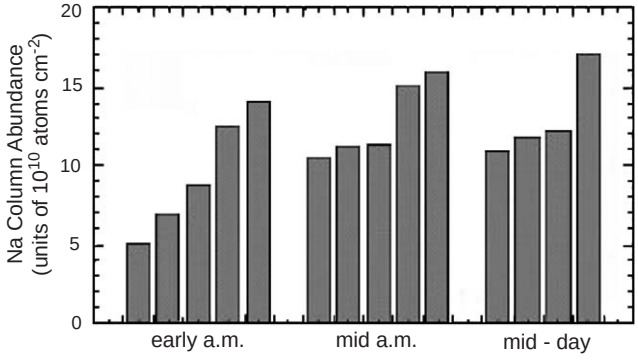

Fig. 6. Slit sector abundances have been divided according to time of day on Mercury to search for any significant variation in abundance. There does appear to be a trend for lower abundances toward the early a.m. sector.

traces along the slit are strongly enhanced at the illuminated limb and the largest column abundances are also observed close to the illuminated limb.

Acknowledgements

We wish to thank the TNG personnel for the competent assistance during these difficult observations. This work has been partially supported on the Italian side with a contract from the Ministry of Research and University (MIUR). At Boston University, this work was supported by seed research funds from its Center for Space Physics.

References

Bida, T.A., Killen, R.M., Morgan, T.H., 2000. Discovery of calcium in the Mercury's exosphere. Nature 404, 159–161.

Broadfoot, A.L., Shemansky, D.E., Kumar, S., 1976. Mariner 10—Mercury atmosphere. Geophys. Res. Lett. 3, 577–580.

Chamberlain, J.W., Hunten, D.M., 1987. Theory of planetary atmospheres: an introduction to their physics and chemistry. Int. Geophysics Ser. 36.

Domingue, D.L., Sprague, A.L., Hunten, D.M., 1997. Dependence of mercurian atmospheric column abundance estimations on surface-reflectance modeling. Icarus 128, 75–82.

Hapke, B., 1986. Bidirectional reflectance spectroscopy: 4. The extinction coefficient and the opposition effect. Icarus 67, 264–280.

Hunten, D.M., Sprague, A.L., 1997. Origin and character of the lunar and mercurian atmospheres. Adv. Space Res. 1551–1560.

Hunten, D.M., Wallace, L.V., 1993. Resonance scattering by mercurian sodium. Astrophys. J. 417, 757–761.

Hunten, D.M., Roach, F.E., Chamberlain, J.W., 1956. A photometric unit for the airglow and aurora. J. Atmos. Terr. Phys. 8, 345–346.

Hunten, D.M., Morgan, T.H., Shemansky, D.E., 1988. The Mercury Atmosphere, Mercury. University of Arizona Press, pp. 562–612.

Ip, W.H., 1990. On solar radiation-driven surface transport of sodium atoms at Mercury. Astrophys. J. 356, 675–681.

Killen, R.M., Potter, A.E., Fitzsimmons, A., Morgan, T.H., 1999a. Sodium D2 line profiles: clues to the temperature structure of Mercury's exosphere. Planet. Space Sci. 47, 1449–1458.

Killen, R.M., Potter, A.E., Morgan, T.H., 1999b. Spatial distribution of sodium vapor in the atmosphere of Mercury. Icarus 85, 145–167.

Leblanc, F., Johnson, R.E., 2003. Mercury's sodium exosphere. Icarus 164 (2), 261–281.

McGrath, M., Johnson, R.E., Lanzerotti, L.J., 1986. Sputtering of sodium on the planet Mercury. Nature 323, 694–696.

Potter, A.E., Morgan, T.H., 1985. Discovery of sodium in the atmosphere of Mercury. Science 229, 651–653.

Potter, A.E., Morgan, T.H., 1986. Potassium in the atmosphere of Mercury. Icarus 67, 336–340.

Potter, A.E., Morgan, T.H., 1990. Evidence for magnetospheric effects on the sodium atmosphere of Mercury. Science 248, 835–838.

Potter, A.E., Killen, R.M., Morgan, T.H., 1999. Rapid changes in the sodium exosphere of Mercury. Planet. Space Sci. 47, 1441–1448.

Potter, A.E., Killen, R.M., Morgan T.H., 2002. The sodium tail of Mercury. Meteoritics Planetary Sci. 37, 1165–1172.

Smyth, W.H., Marconi, M.L., 1995. Theoretical overview and modelling of the sodium and potassium atmospheres of Mercury. Astrophys. J. 441, 839–864.

Sprague, A.L., 1992. Mercury's atmospheric sodium bright spots: A possible cause. JGR 97 (Ell), 257–264.

Sprague, A.L., Kozlowski, R.W.H., Hunten, D.M., Schneider, N.M., Domingue, D.L., Wells, W.K., Schmitt, W., Fink, U., 1997. Distribution and abundance of sodium in mercury's atmosphere, 1985–1988. Icarus 129, 506–527.

Sprague, A.L., Schmitt, W.J., Hill, R.E., 1998. Mercury: sodium atmospheric enhancements, radar-bright spots and visible surface features. Icarus 136, 60–68.